Spin Electronics

Influence of Intrinsic Thermal Stability on Switching Rate and Tunability of Dual-Biased Magnetic Tunnel Junctions for Probabilistic Bits

Brandon R. Zink and Jian-Ping Wang*

Department of Electrical and Computer Engineering, University of Minnesota, Minneapolis, MN 55455, USA
* *Fellow, IEEE*

Received 24 Mar 2021, revised 26 Apr 2021, accepted 5 May 2021, published 28 May 2021, current version 17 Jun 2021.

Abstract—Recently, magnetic tunnel junctions (MTJs) with superparamagnetic free layers (sMTJs) have been proposed as key components in probabilistic bits (p-bits). However, the average fluctuation rates of sMTJs are very sensitive to slight variations in the device dimensions, which creates a major obstacle to their realization in large-scale networks. One possible solution is to implement dual-biasing on p-bits to offset the effects of variations through onboard corrections. In our previous work, we demonstrated that dual-biasing has the unique capability of separate control over the high- and low-state dwell times, which adds an extra degree of tunability in the signals generated. However, these studies investigated dual-biasing on thermally stable MTJs; therefore, the maximum switching rates were lower than the gigahertz rates desired for sMTJ-based p-bit circuits. While dual-biasing on sMTJs rather than thermally stable MTJs would improve the switching rates, some of the flexibility and robustness of dual-biasing may be sacrificed due to the sensitivity of sMTJs. In this letter, we applied the dual-biasing method on 10 MTJs with varying thermal stability factors to test if sMTJs can achieve the same degree of separation between high- and low-state dwell-time tunability as thermally stable MTJs. Our results show that two degrees of tunability was achieved on all MTJs tested, thus demonstrating that dual-biased p-bits can achieve switching rates equal to or greater than single-biased sMTJs.

Index Terms—Spin electronics, magnetic tunnel junctions, spin torque, thermal stability, tunneling magnetoresistance.

I. INTRODUCTION

Spintronic devices provide many unique functionalities to achieve novel computing architectures and schemes [Wang 2017]. Probabilistic spin logic (**PSL**) has emerged in recent years as a promising solution for various low-energy cognitive computing tasks [Camsari 2018, Faria 2018, Sutton 2017, Zand 2018]. The elementary computing units of PSL circuits are thermally unstable, stochastic devices called probabilistic bits (**p-bit**s). Many p-bit designs propose magnetic tunnel junctions (**MTJ**s) with a superparamagnetic free layer (**sMTJ**) as key components [Borders 2019, Faria 2017]. For sMTJs, thermal fluctuations alone can drive magnetization switching between the antiparallel (**AP**) and parallel (**P**) states due to their low intrinsic thermal stability factor (Δ_0). The output of a p-bit is defined by the averaged resistance of the MTJ, which can be controlled with an applied voltage or current [Ostwal 2019, Parks 2020].

A promising strategy for designing sMTJs is to use circular MTJs with in-plane anisotropy [Debashis 2018]. According to the Néel–Brown model, thermal fluctuations could drive MTJs with $\Delta_0 \approx 0$ to switching rates of 1–10 GHz [Lopez-Diaz 2002]. However, the switching rate and transfer curves of sMTJs are extremely sensitive to variations in device dimensions, which creates a major obstacle for their implementation in large-scale p-bit networks [Abeed 2019].

One possible solution to avoid the effects of device variations is an external biasing scheme, which we refer to as "dual-biasing." This method generates stochastic switching signals from MTJs using an external magnetic field (H_{bias}) and a dc voltage (V_{bias}) with specific restrictions on their magnitudes and orientations. In our previous work, we showed that average dwell times could be tuned over four orders of magnitude with dual-biasing [Zink 2018, Zink 2019]. We also carried out a hardware feasibility demonstration of p-bits using a dual-biasing scheme [Lv 2019]. The most unique capability of dual-biasing is that the average AP- and P-state dwell times could be tuned separately with H_{bias} and V_{bias}, respectively. This two-degrees-of-tunability feature means that the average output and switching rate of these signals can be controlled separately, making dual-biasing a potential solution of avoiding the effects of variations in device sizes through onboard corrections.

Our previous work on dual-biasing only examined signals generated from thermally MTJs (where $\Delta_0 \geq 25$). These studies demonstrated that dual-biasing is compatible with the existing state-of-the-art magnetoresistive random access memory technology; however, the maximum switching rates achieved were lower than the ideal gigahertz switching rates desired for p-bits. Therefore, for dual-biasing to be a realistic prospect in p-bit circuits, MTJs with lower Δ_0 will be required; however, one potential concern is that dual-biasing will not achieve the same degree of tunability on thermally unstable MTJs, due to their sensitivity to noise and defects. In this letter, we apply the dual-biasing method on 10 MTJs with Δ_0 varying from 10.5 to 35.6. For each device, we analyze the switching speed, average output, as well as the degree of separation between AP- and P-state dwell-time tunability. In our analysis, we investigate all the tradeoffs of dual-biasing on sMTJs to determine if two degrees of tunability is still achieved.

Corresponding authors: Jian-Ping Wang and Brandon R. Zink (e-mail: jpwang@umn.edu; zinkx030@umn.edu).
Digital Object Identifier 10.1109/LMAG.2021.3084901

Table 1. Intrinsic Properties and Category of all MTJs Tested

Category	MTJ no.	Δ_0	R_P (Ω)	H_C (Oe)	Nominal dimensions (nm^2)
Super-paramagnetic MTJs (sMTJs)	**1**	**10.5**	**1360**	**NA**	**120 x 40**
	2	**11.4**	**1330**	**NA**	**120 x 40**
	3	**12.0**	**1100**	**NA**	**120 x 50**
Thermally unstable MTJs	4	19.0	1290	NA	130 x 45
	5	18.8	1015	NA	120 x 50
Semi-stable MTJs	**6**	**24.9**	**1260**	**11**	**130 x 45**
	7	**26.4**	**1090**	**11**	**120 x 50**
	8	**28.2**	**1250**	**21**	**120 x 45**
Thermally stable MTJs	9	34.2	570	15	130 x 60
	10	35.6	620	20	130 x 60

II. EXPERIMENT

The MTJs tested are elliptical nanopillars with in-plane anisotropy and a stack structure of PtMn(15)/SAF/MgO(0.8)/$Co_{60}Fe_{20}B_{20}$(2.0), where layer thicknesses are in nanometers. SAF is the synthetic antiferromagnetic fixed layer, which consists of $Co_{70}Fe_{30}$(2.5)/Ru(0.85)/$Co_{40}Fe_{40}B_{20}$(2.4). Each MTJ has a resistance–area product of 3.5 $\Omega\cdot\mu m^2$ and a tunneling magneto-resistance (**TMR**) ratio between 135% and 150%.

Table 1 lists the intrinsic thermal stability factors (Δ_0), P-state resistances (R_P), coercivities (H_C), and nominal dimensions for all 10 MTJs. For each device, R_P was obtained from its resistance versus field (R–H) plots, examples of which are shown in Fig. 1(a) and (b). Additionally, for MTJs with well-defined switching fields, R–H plots can be used to measure H_C as well as the stray field of the MTJ (H_{stray}), as illustrated in Fig. 1(a). Some MTJs fluctuated randomly between AP and P-states at fields near H_{stray}, as seen in Fig. 1(b); therefore, there is no H_C for these devices.

The nominal dimensions are presented as long-axis diameter × short-axis diameter. One approach to ensuring wide variability in Δ_0 among the MTJs tested is to vary the aspect ratio (long-axis to short axis dimension) among the devices during fabrication. However, Table 1 shows that R_P and H_C often varied significantly between MTJs with the same nominal dimensions. This indicates that the actual device dimensions deviated from their nominal ones. For this reason, we ensured variability in Δ_0 among the MTJs based on R_P and H_C measurements rather than nominal dimensions.

Switching probability (P_{SW}) measurements were used to calculate Δ_0. Synchronized P_{SW} measurements were used on MTJs, whose R–H curves showed clear hysteresis (MTJs 6–10). For these MTJs, we obtained multiple P_{SW} distribution curves at $H_{bias} = H_{stray}$ and pulsewidths $\geq$ 500 ns, then calculate Δ_0 from the thermal activation model as was done by Heindl [2011]. The R–H curves for MTJs 1–5 showed that these devices randomly fluctuated between the AP and P-states at H_{bias} near the switching fields. Therefore, Δ_0 was calculated using asynchronous time-domain data from the random telegraphic signals generated by these devices as was done by Piotrowski [2016]. Fig. 1(b) illustrates that R–H data can only provide an approximation of H_{stray} for these devices; therefore, these measurements were collected at multiple sets with slightly varying H_{bias}; all were $\approx H_{stray}$.

In our analysis, we divided these 10 MTJs into four categories, which were 1) sMTJs, 2) unstable MTJs, 3) semistable MTJs, and 4) stable MTJs. The reason for choosing four categories was based on how the MTJs seemed to cluster into four groups in terms of their Δ_0 values. Even though both sMTJs and unstable MTJs exhibited superparmagnetic behavior (as shown in the asynchronous P_{SW} measurements as well as their R–H plots), they are placed into separate categories because the retention time is ~2 orders of magnitude lower for the sMTJs than for the unstable MTJs. Similarly, semistable MTJs and stable MTJs are placed into separate categories because the retention time of the semistable MTJs is ~4 orders of magnitude higher than those for stable MTJs.

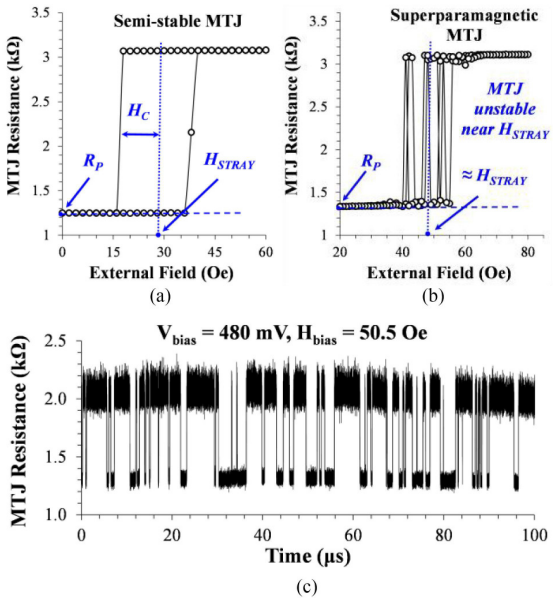

Fig. 1. Resistance versus field plots for (a) MTJ 6 and (b) MTJ 2 (see Table 1). (c) Random telegraphic switching signals generated by MTJ 2 under a bias field of 50.5 Oe (relative to H_{stray}) and a bias voltage of 480 mV.

Dual-biasing measurements were collected for each MTJ using the same experimental setup described in our previous work [Zink 2018]. Note that these dual-biasing measurements are not the same as the asynchronous P_{SW} measurements used to calculate Δ_0 for MTJs 1–5 since dual-biasing has specific parameters on H_{bias} and V_{bias}. The polarity of the biases should be set so that H_{bias} favors P-state orientation and V_{bias} favors AP-state orientation. For our purposes, H_{bias} is said to increase as it moves to stronger P-state orientation, which occurs when $H_{bias} \leq H_{stray}$ [recall Fig. 1(a) and (b)]. All H_{bias} values are presented relative to the MTJ's H_{stray}. Certain combinations of magnitudes for V_{bias} and H_{bias} produce a condition where the MTJ is never in the energetically favorable state, which causes continuous toggling between the AP- and P-states, thus generating random telegraphic switching signals, as illustrated in Fig. 1(c). The physical mechanisms which produce high levels of tunability and control are explained in greater detail in our previous work [Zink 2019].

III. RESULTS

A. Transfer Characteristics

In our analysis, we defined the time-averaged output as the percentage of time the MTJ spends in the AP-state, which we refer to as the AP-rate. AP-rate versus V_{bias} curves were acquired for all MTJs,

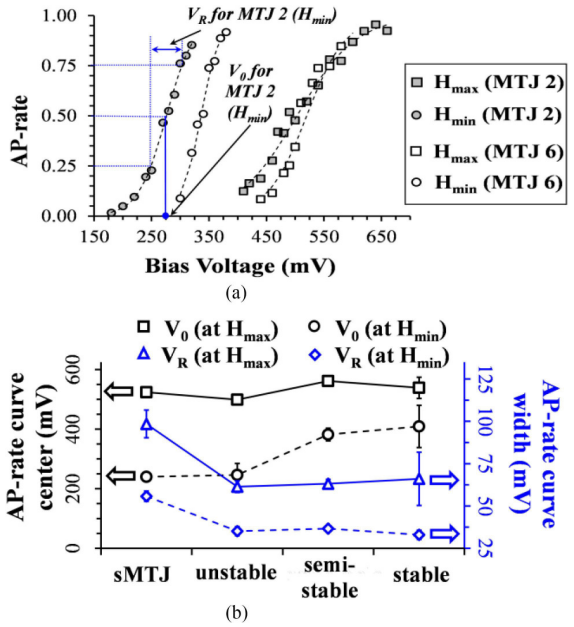

Fig. 2. (a) AP-rate versus bias voltage curves at H_{min} and H_{max} for a semistable MTJ and an sMTJ (MTJs 6 and 2 from Table 1). H_{min} = 60 Oe and 30.5 Oe, and H_{max} = 80 Oe and 55.5 Oe for MTJ 6 and 2, respectively. (b) Line plots showing the center (V_0) and width (V_R) of the voltage-dependent transfer curves for each MTJ category at H_{min} and H_{max}.

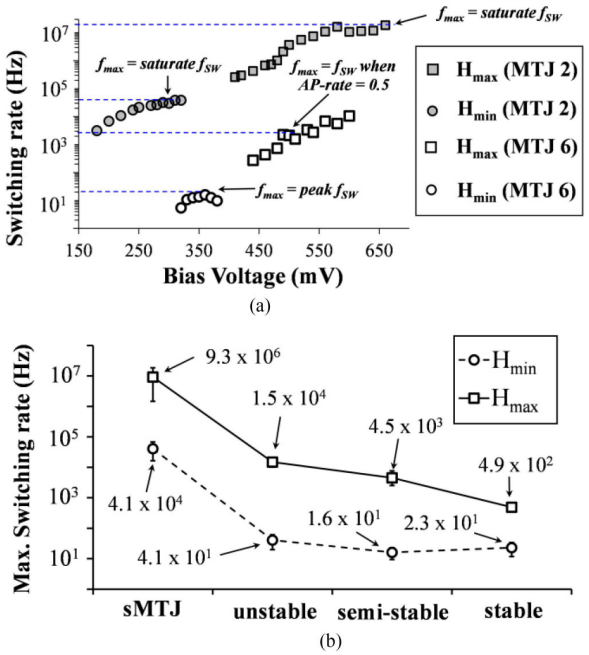

Fig. 3. (a) Dependence of average switching rate with bias voltage at H_{max} and H_{min} for MTJs 6 and 2 (see Table 1). (b) Maximum switching rate (f_{max}) achieved for each MTJ category.

examples of which are shown in Fig. 2(a). These curves represent the transfer properties of the device and were characterized in terms of their center and width (V_0 and V_R, respectively) where V_0 is defined as V_{bias} when AP-rate = 0.5 V_R is defined as the difference in V_{bias} at AP-rates of 0.75 and 0.25. V_0 and V_R were obtained by fitting the AP-rate curves to a hyperbolic tangent function as was done in our previous work (see Zink [2019]).

The line plots of the average V_0 and V_R measured at both minimum and maximum H_{bias} (H_{min} and H_{max}, respectively) are shown in Fig. 2(b) for each MTJ category. These data show that V_0 increases as Δ_0 increases at H_{min}, where $V_0 = 240 \pm 15$ mV for sMTJs and 409 ± 71 mV for stable MTJs. However, at H_{max}, V_0 is nearly constant between all sets, where $V_0 = 524 \pm 11$ mV for sMTJs and 539 ± 36 mV for stable MTJs. This cutoff in V_0 can be attributed to the rectifying properties of MTJs, where V_{bias} causes their TMR ratio to decrease. This creates an upper limit on V_{bias} for the dual-biasing method since it relies on current fluctuations caused by resistance changes [Zink 2019]. Therefore, the limiting factor for V_{bias} is the TMR ratio and not Δ_0, which is why V_0 is not dependent on Δ_0 at H_{max} in Fig. 2(b).

For all MTJs, V_R increased from H_{min} to H_{max}. Note that if H_{bias} were equal among all MTJs, then V_R would decrease as Δ_0 increases. However, larger H_{bias} was needed for MTJs with larger Δ_0, thus increasing V_R, which explains why V_R appears to be equal among unstable, semistable, and stable MTJs. However, V_R was at least two times larger for sMTJs at both H_{min} and H_{max}, despite smaller H_{bias}.

In terms of transfer curve characteristics, sMTJs showed superior performance to all others. Not only do they require lower minimum V_0 compared to the other three categories, but they also have the same maximum V_0 values, thus providing a larger tunability range. Furthermore, sMTJs had significantly wider transfer curves than the others, which are ideal for p-bits since output resolution and noise tolerance improve with transfer curve width.

B. Average Switching Rate

For every dataset, we measured the average AP- and P-state dwell times (τ_{AP} and τ_P, respectively) which were used to calculate the average switching rate (f_{SW}) using $f_{SW} = (\tau_{AP} + \tau_P)^{-1}$. Fig. 3(a) shows f_{SW} plotted with V_{bias} for MTJs 2 and 6 (see Table 1) at H_{min} and H_{max}. This figure illustrates three different behaviors of f_{SW} with V_{bias}. One is that f_{SW} reaches a maximum and then decreases, which is seen at H_{min} for MTJ 6. The second is that f_{SW} increases with V_{bias} until reaching a saturation point, as seen at H_{max} and H_{min} for MTJ 2. Lastly, f_{SW} increases exponentially with V_{bias}, as seen at H_{max} for MTJ 6.

Here, we analyze the maximum f_{SW} (f_{max}) achieved at H_{min} and H_{max} for all MTJs. The method of calculating f_{max} depended on the behavior of f_{SW} versus V_{bias}. If f_{SW} peaked or saturated, then f_{max} was simply f_{SW} at the peak or saturation value. However, if f_{SW} increases exponentially with V_{bias}, then defining f_{max} was not as straightforward since f_{max} may occur when AP-rate > 0.9, which is not particularly useful for p-bit applications. Therefore, for these datasets, we defined f_{max} as f_{SW} when the AP-rate = 0.5.

Fig. 3(b) shows a line plot of f_{max} at H_{min} and H_{max} for all four categories. Unsurprisingly, f_{max} was the largest for sMTJs, which achieved $f_{max} \approx 10^4$–10^7 Hz. The remaining three MTJ categories showed $f_{max} \approx$ 10–100 Hz at H_{min}. This is because time-domain data were not collected if the dwell times > 50 ms, due to bandwidth limitations. For sMTJs and unstable MTJs, f_{max} at H_{min} is on the same order of magnitude as their intrinsic dwell times whereas semistable and stable MTJs required larger biases to reach 10 Hz. The upper limit of V_{bias} for all MTJs [recall Fig. 2(b)] means that f_{max} at H_{max} is the

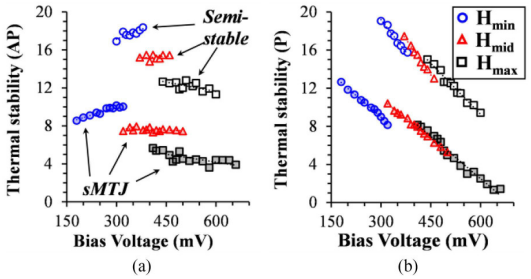

Fig. 4. Effective thermal stability factor versus bias voltage at H_{max}, H_{min}, and H_{mid} for (a) AP-state and (b) P-state components for MTJs 6 and 2 (see Table 1). Note that $H_{mid} = 70$ Oe for MTJ 6 and 45.5 Oe for MTJ 2.

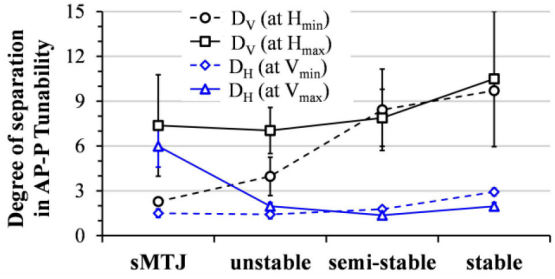

Fig. 5. Degree of separation between Δ_{AP} and Δ_P tunability with voltage and field (D_V and D_H, respectively) for each MTJ category. D_V represents the order of magnitude decrease in τ_P for every 1 order of magnitude increase in τ_{AP}, and D_H represents the order of magnitude decrease in τ_{AP} for every 1 order of magnitude increase in τ_P.

upper limit of f_{max} of the MTJ, meaning unstable MTJs and sMTJs have a broader tuning range of f_{max} than semistable and stable MTJs.

C. Degree of Separation Between Δ_{AP} and Δ_P Tunability

For this analysis, τ_{AP} and τ_P were used to calculate the AP- and P-state components of the effective thermal stability factors (Δ_{AP} and Δ_P, respectively) using the Néel–Arrhenius equation, $\tau_{AP(P)} = \tau_0 \exp(\Delta_{AP(P)})$, where the inverse attempt frequency (τ_0) was assumed to be 1 ns [Lopez-Diaz 2002]. Fig. 4(a) and (b) shows Δ_{AP} and Δ_P plotted with V_{bias} for MTJs 6 and 2 (see Table 1) at H_{min}, H_{max}, and a bias field between H_{min} and H_{max}, referred to as H_{mid}. For both MTJs, Δ_{AP} increases with V_{bias} and decreases with H_{bias} whereas Δ_P decreases with V_{bias} and increases with H_{bias}. However, two-degrees-of-tunability capability of dual-biasing is revealed when investigating the relative changes in Δ_{AP} versus Δ_P with both V_{bias} and H_{bias}. At H_{min}, changes in Δ_P with V_{bias} are $\sim$3.5$\times$ larger than changes in Δ_{AP} for MTJ 6 and $\sim$2$\times$ larger for MTJ 2. At H_{max}, changes in Δ_P with V_{bias} are $\sim$6$\times$ and 4.5$\times$ larger than the changes in Δ_{AP} for MTJs 6 and 2, respectively. In fact, Δ_{AP} appears to decrease slightly with V_{bias} as H_{bias} increases, which was observed for all devices tested and explained in our previous work [Zink 2019]. This means that P-state pulsewidths will decrease by 2–3 orders of magnitude while AP-state pulsewidths do not even change by 1 order. On the other hand, at the minimum voltages (V_{min}), changes in Δ_{AP} with H_{bias} are $\sim$1.5$\times$ and 2.5$\times$ larger than changes in Δ_P and at V_{max}, $\sim$9.5$\times$ and 2$\times$ for MTJs 2 and 6, respectively. This means that that AP-state pulsewidths decrease with H_{bias} by $\approx$ 2–2.5 orders of magnitude while P-state pulsewidths increase by less than 1. The influences of H_{bias} and V_{bias} on Δ_{AP} and Δ_P observed in Fig. 4(a) and (b) were also observed in our previous work [Zink 2018, 2019], which demonstrates the reproducibility of dual-biasing.

Note that Δ_{AP} and Δ_P are influenced by both V_{bias} and H_{bias} to some degree; therefore, the two-degrees-of-tunability feature can be quantified. In our analysis, this is done using a metric we refer to as the degree of separation in Δ_P and Δ_{AP} tunability, which we divided into V_{bias} dependence and H_{bias} dependence components (D_V and D_H, respectively). D_V and D_H are expressed using slopes of Δ_P and Δ_{AP} with V_{bias} and H_{bias}, respectively, as seen in (1). D_V represents the order of magnitude decrease in τ_P for every 1 order of magnitude increase in τ_{AP} with V_{bias}. Similarly, D_H represents the order of magnitude decrease in τ_{AP} for every 1 order of magnitude increase in τ_P with H_{bias}. According to the Néel–Brown model [Li 2004], $\Delta_{AP(P)}$ is proportional

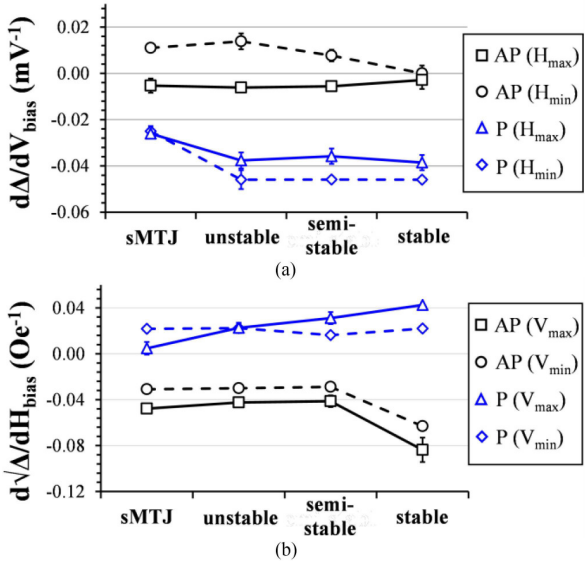

Fig. 6. Slopes Δ_{AP} and Δ_P with respect to (a) V_{bias} and (b) H_{bias} for each MTJ category.

to $H_{bias}{}^2$; therefore, we defined D_H in terms of changes in $\sqrt{\Delta_{AP(P)}}$

$$D_V = \left| \frac{d\Delta_P / dV_{bias}}{d\Delta_{AP} / dV_{bias}} \right| \quad D_H = \left| \frac{d\sqrt{\Delta_{AP}} / dH_{bias}}{d\sqrt{\Delta_P} / dH_{bias}} \right|. \tag{1}$$

The line plots in Fig. 5 show D_V and D_H for all four MTJ categories. D_V is calculated at both H_{min} and H_{max}, and D_H is calculated at both V_{min} and V_{max}. This plot shows that D_V clearly improves as Δ_0 increases at H_{min}. However, the influence of Δ_0 on D_V at H_{max} is unclear due to the large error bars. One key observation is that D_V improves from H_{min} to H_{max} for sMTJs and unstable MTJs, whereas D_V does not change significantly with H_{bias} for semistable and stable MTJs. Fig. 6 shows that dual-biasing on stable MTJs achieves better degree of separation in tunability with V_{bias} since D_V maintains a value above 6 from H_{min} to H_{max}. It should be noted that $D_V > 2$ for sMTJs at H_{min}, meaning that the two-degrees-of-tunability capability is still present.

The D_H curves in Fig. 5 shows that the MTJ category, which produces the largest D_H, is dependent on V_{bias}. These curves show that stable MTJs have the largest D_H at V_{min} whereas sMTJs have the largest D_H at V_{max}. This result demonstrates that even though the degree of separation in Δ_P tunability with V_{bias} is reduced in sMTJs, two degrees

of tunability is not sacrificed since their degree of separation in Δ_{AP} tunability with H_{bias} improves.

The behavior of D_V and D_H can be explained using the line plots in Fig. 6(a) and (b), which show the slopes of Δ_{AP} and Δ_P with V_{bias} and H_{bias}, respectively. Fig. 7(a) shows that $d\Delta_{AP}/dV_{bias}$ is $\sim 10\times$ larger for sMTJs and unstable MTJs than for stable MTJs at H_{min}, which clearly illustrates why D_V is significantly smaller in sMTJs compared to stable MTJs. Furthermore, $|d\Delta_P/dV_{bias}|$ is $\sim 2\times$ lower for sMTJs than for all other categories at both H_{min} and H_{max}, which also contributes to a reduction in D_V for sMTJs. The key observation from Fig. 7(a) is that $d\Delta_{AP}/dV_{bias}$ changes sign from H_{min} to H_{max} for all MTJs. This was also observed in one of our previous studies where we attributed this sign change to the influence of H_{bias} on the AP- and P-state components of the intrinsic critical switching voltage (V_{C0}), where increasing H_{bias} caused dV_{C0}/dV_{bias} to increase in the AP-state but not in the P-state [Zink 2019]. This sign change suggests that each MTJ, regardless of Δ_0, has a bias field where $d\Delta_{AP}/dV_{bias} \approx 0$, resulting in a near infinite D_V. Note that this change in sign in $d\Delta_{AP}/dV_{bias}$ explains the large error bars for D_V at H_{max} in Fig. 5.

This result may seem like an exciting prospect for complete independent tuning of Δ_P and Δ_{AP}. However, the dual-biasing method requires tuning of both V_{bias} and H_{bias}, meaning that optimum control over Δ_P and Δ_{AP} occurs when $d\Delta_{AP}/dV_{bias}$ has minimal dependence on H_{bias} over a large range of bias fields. Our results show that the stable MTJs had the largest D_V values and smallest variation in $d\Delta_{AP}/dV_{bias}$ from H_{min} to H_{max}. It should be noted that the VCMA efficiency increases as MTJ size decreases [Piotrowski 2016]. In this letter, sizes of the stable MTJs are larger than the sMTJs, as seen in the R_P values in Table 1. Therefore, the weak dependence of $d\Delta_{AP}/dV_{bias}$ on H_{bias} seen in stable MTJs may be a result of device size and not Δ_0.

Fig. 6(b) shows that $|d\sqrt{\Delta_{AP}}/dH_{bias}|$ is ~ 2–$3\times$ larger for stable MTJs than all other MTJs at both V_{min} and V_{max}. Since $d\sqrt{\Delta_P}/dH_{bias}$ is nearly constant among all MTJs at V_{min}, D_H is largest for stable MTJs at V_{min}. However, each MTJ category had showed different responses of $d\sqrt{\Delta_P}/dH_{bias}$ with V_{bias}. From V_{min} to V_{max}, $d\sqrt{\Delta_P}/dH_{bias}$ decreased significantly for sMTJs, remained constant for unstable MTJs, and increased for semistable and stable MTJs. The change in $d\sqrt{\Delta_P}/dH_{bias}$ from V_{min} to V_{max} is partially due to the influence of V_{bias} on the anisotropy field (H_K) and V_{C0}. Previous experimental work has shown that VCMA efficiency increases as the MTJs thermal stability factor increases [Piotrowski 2016], which explains the differences in responses of $d\sqrt{\Delta_P}/dH_{bias}$ since the influence of V_{bias} on $d\sqrt{\Delta_P}/dH_{bias}$ in stable MTJs is primarily characterized by dH_K/dV_{bias} and dV_{C0}/dV_{bias}. This discrepancy in the behavior of $d\sqrt{\Delta_P}/dH_{bias}$ with V_{bias} explains why D_H is largest for sMTJs at V_{max}.

IV. CONCLUSION

A major challenge in realizing p-bits in large-scale PSL circuits is that any deviations in Δ_0 between MTJs will result in significant differences in their transfer curves and switching rates, resulting in computation errors and bottlenecks. Dual-biasing is a promising solution for correcting these variations as it provides a method for tuning the center and width of the p-bits transfer curve as well as its switching rate. In our previous studies, the dual-biasing technique was applied to thermally stable MTJs, therefore sacrificing switching rate for two degrees of tunability. However, in this letter, we demonstrated that dual-biasing can achieve two degrees of tunability for both sMTJs and stable MTJs. Even though sMTJs did not achieve the same degree of separation in low-state tunability with voltage, the capability for two degrees of tunability was not sacrificed. Additionally, dual-biased sMTJs improved several other performance metrics such as larger degree of separation in high-state tunability with field, enhanced control over average output and switching rate, and better noise immunity in transfer curves.

ACKNOWLEDGMENT

This work was supported in part by the Center for Probabilistic Spin Logic for Low-Energy Boolean and Non-Boolean Computing, one of the Nanoelectronic Computing Research centers as task 2759.001, and in part by the Semiconductor Research Corporation program sponsored by the National Science Foundation under Grant 1739635. The authors thank Dr. Yang Lv for useful disscussion.

REFERENCES

Abeed M A, Bandyopadhyay (2019), "Low energy nanomagnet design for binary stochastic neurons: Design challenges for real nanomagnets with fabrication defects," *IEEE Magn. Lett.*, vol. 10, 4504405, doi: 10.1109/LMAG.2019.2929484.

Borders W A, Pervaiz A Z, Fukami S, Camsari K Y, Ohno H, Datta S (2019), "Integer factorization using stochastic magnetic tunnel junctions," *Nature*, vol. 573, pp. 390–393, doi: 10.1038/s41586-019-1557-9.

Camsari K Y, Sutton B M, Datta S (2018), "p-bits for probabilistic spin logic," *Appl. Phys. Rev.*, vol. 6, 011305, doi: 10.1063/1.5055860.

Debashis P, Faria R, Camsari K Y, Chen Z (2018), "Design of stochastic nanomagnets for probabilistic spin logic," *IEEE Magn. Lett.*, vol. 9, 4305205, doi: 10.1109/LMAG.2018.2860547.

Faria R, Camsari K Y, Datta S (2017), "Low-barrier nanomagnets as p-bits for spin logic," *IEEE Magn. Lett.*, vol. 8, 4105305, doi: 10.1109/LMAG.2017.2685358.

Faria R, Camsari K Y, Datta S (2018), "Implementation of Bayesian networks with embedded stochastic MRAM," *AIP Adv.*, vol. 8, 045101, doi: 10.1063/1.5021332.

Heindl R, Rippard W H, Russek S E, Pufall M R, Kos A B (2011), "Validity of the thermal activation model for spin-transfer torque switching in magnetic tunnel junctions," *J. Appl. Phys.*, vol. 109, 073910, doi: 10.1063/1.3562136.

Li Z., Zhang S. (2004), "Thermally assisted magnetization reversal in the presence of a spin transfer torque," *Phys. Rev. B*, vol. 69, 134416, doi: 10.1103/PhysRevB.69.134416.

Lopez-Diaz L, Torres L, Moro E (2002), "Transition from ferromagnetism to superparamagnetism on the nanosecond time scale," *Phys. Rev. B*, vol. 65, 224406, doi: 10.1103/PhysRevB.65.224406.

Lv Y, Bloom R, Wang J-P (2019), "Experimental demonstration of probabilistic spin logic by magnetic tunnel junctions," *IEEE Magn. Lett.*, vol. 10, 4510905, doi: 10.1109/LMAG.2019.2957258.

Ostwal V, Appenzeller J (2019), "Spin-orbit torque-controlled magnetic tunnel junction with low thermal stability for tunable random number generation," *IEEE Magn. Lett.*, vol. 10, 4503305, doi: 10.1109/LMAG.2019.2912971.

Parks B, Abdelgawad A, Wong T, Evans R, Majetich S A (2020), "Magnetoresistance dynamics in superparamagnetic Co–Fe–B nanodots," *Phys. Rev. Appl.*, vol. 13, 014063, doi: 10.1103/PhysRevApplied.13.014063.

Piotrowski S K, Bapna M, Oberdick S D, Majetich S A (2016), "Size and voltage dependence of effective anisotropy in sub-100-nm perpendicular magnetic tunnel junctions," *Phys. Rev. B*, vol. 94, 014404, doi: 10.1103/PhysRevB.94.014404.

Sutton B, Camsari K Y, Behin-Aein B, Datta S (2017), "Intrinsic optimization using stochastic nanomagnets," *Sci. Rep.*, vol. 7, 44370, doi: 10.1038/srep44370.

Wang J-P, Sapatnekar S S, Kim C H, Crowell P, Koester S, Datta S, Roy K, Raghunathan, Hu W S, Niemier M, Naeemi A, Chien C-L, Ross C, Kawakami R (2017), "A pathway to enable exponential scaling for the beyond-CMOS era: Invited," in *Proc. 54th Annu. Des. Automat. Conf.*, pp. 1–6, doi: 10.1145/3061639.3072942.

Zand R, Camsari K Y, Pyle S D, Ahmed I, Kim C H, Demara R F (2018), "Low-energy deep belief networks using intrinsic sigmoidal spintronic-based probabilistic neurons," in *Proc. Great Lakes Symp. VLSI,* pp. 15–20, doi: 10.1145/3194554.3194558.

Zink B R, Lv Y, Wang J-P (2018), "Telegraphic switching signals by magnetic tunnel junctions for neural spiking signals with high information capacity," *J. Appl. Phys.*, vol. 124, 152121, doi: 10.1063/1.5042444.

Zink B R, Lv Y, Wang J-P (2019) "Independent control of antiparallel- and parallel-state thermal stability factors in magnetic tunnel junctions for telegraphic signals with two degrees of tunability," *IEEE Trans. Electron Devices*, vol. 66, pp. 5353–5359, doi: 10.1109/TED.2019.2948218.